The development of high quality seals for silicon patch-clamp chips.

Thomas Sordel, Frédérique Kermarrec, Yann Sinquin, Isabelle Fonteille, Michel Labeau, Fabien Sauter-Starace, Catherine Pudda, François de Crécy, François Chatelain, Michel de Waard, et al.

The development of high quality seals for silicon patch-clamp chips

Sordel T[a], Kermarrec F[a], Sinquin Y[a], Fonteille I[a], Labeau M[c], Sauter-Starace F[b], Pudda C[b], de Crécy F[b], Chatelain F[a], De Waard M[d] , Arnoult C[d], Picollet-D'hahan N[a,*].

[a]CEA, DSV, iRTSV/Biopuces, 17 rue des Martyrs F-38054 Grenoble Cedex 9, France ; [b]CEA, Leti, 17 rue des Martyrs F-38054 Grenoble Cedex 9, France; [c]LMGP/INPG-Minatec, 3 Parvis Louis Néel, BP257-38016 Grenoble, France; [d]INSERM U836, Institut des Neurosciences de Grenoble, Site Santé Tronche, 38042 Grenoble Cedex 09, France.

[*] Corresponding author: nathalie.picollet-dhahan@cea.fr ; Tel : + 33 4 38 78 67 78 ; fax : + 33 4 38 78 59 17.

Running title: silicon patch-clamp chip surface investigation

ABSTRACT

Planar patch-clamp is a two-dimensional variation of traditional patch-clamp. By contrast to classical glass micropipette, the seal quality of silicon patch-clamp chips (i.e. seal resistance and seal success rate) have remained poor due to the planar geometry and the nature of the substrate and thus partially obliterate the advantages related to planar patch-clamp. The characterization of physical parameters involved in seal formation is thus of major interest. In this paper, we demonstrate that the physical characterization of surfaces by a set of techniques (Atomic Force Microscopy (AFM), Scanning Electron Microscopy (SEM), X-ray Photoelectron Spectroscopy (XPS), surface energy (polar and dispersive contributions), drop angles, impedance spectroscopy, combined with a statistical design of experiments (DOE)) allowed us discriminating chips that provide relevant performances for planar patch-clamp analysis. Analyses of seal quality demonstrate that dispersive interactions and micropore size are the most crucial physical parameters of chip surfaces, by contrast to surface roughness and dielectric membrane thickness. This multi-scale study combined with electrophysiological validation of chips on a diverse set of cell-types expressing various ion channels (IRK1, hERG and $hNa_v1.5$ channels) unveiled a suitable patch-clamp chip candidate. This original approach may inspire novel strategies for selecting appropriate surface parameters dedicated to biochips.

Keywords: planar patch-clamp; silicon chips; AFM; XPS; impedance; surface energy; ion channels.

1. Introduction

In response to the industrial demand for drug screening on ion channels, most developments today prefer chip-based devices [1, 2]. Development of cell-on-chip-based micro-systems often requires detailed knowledge of the cell/substrate interactions [3-5]. In particular in the field of electrophysiological cell-based devices, a highly resistive cell to chip contact remains the heart of the system and is mandatory for the quality of the electrical recordings. Producing a planar version of gigaseal patch clamping is motivated by the need for automation, parallelization and high throughput cellular electrophysiology [6].

While planar patch-clamp is an established technology, the efficiency and stability of the seals remains a critical bottleneck. The seal success rate on planar-based devices is highly dependent on technologies [7], on the biological quality of the cell suspension and on the investigated cell type [8-10].

In this manuscript, we investigate the critical chip parameters that influence the seal success rate required for ionic recordings. Our aim is to optimize and standardise the industrial process for silicon chip manufacturing and therefore reduce seal rate variability (typically between 50 and 90% today [10]). Silicon was chosen in this study instead of glass or polymers because it is the most versatile substrate today offering high flexibility of microstructuration and surface functionalization [9].

The empirical knowledge acquired from conventional patch-clamp has oriented the selection of the ‘optimal’ planar surface for seal formation. For example, rough edges were previously reported to prevent adequate seal formation, leading some authors to claim that great care should be taken to obtain, as for glass pipette, a clean and smooth surface around the micropore [11, 12]. Moreover, hydrophobic polymer surfaces were not expected to favour a strong interaction with hydrophilic parts of cell membranes [12]. However, since a simple

planar aperture is quite different from pipette tip architecture, we questioned that this empirical knowledge could be transferred to micro-holes on chips. In previous work, we reported the influence of different glass and silicon coatings on cell adhesion and morphology [13]. We also demonstrated the benefit of a Plasma Enhanced Chemical Vapour Deposition (PECVD) SiO_2 coating on seal frequency and quality [14]. It was assumed that the "hourglass" shape of the aperture with a PECVD coating could provide larger sidewalls and/or smoother angles of the micropore and therefore a better contact area between the cell membrane and the substrate. Besides, this funnel-like aperture approach was recently reproduced on plane glass [15] and on boron-doped silicon devices [16]. Following the example of the aperture size diameter, other major parameters such as the shape, depth of the micropore as well as the surface chemistry and topology (roughness and energy) could also dramatically influence seal quality. Current research publishes only qualitative considerations such as "seal rules" or "seal recipes" and not much scale or quantitative values are reported. More specifically for silicon devices, only little systematic comparative studies of chip properties focused on seal quality have been carried out in a planar patch-clamp application [16]. However, in this latter report [16] mean seal resistances still remain limited to 200 MΩ providing a yield of successful recordings very low and inadequate for pharmacological tests and more developed drug-response analyses.

In the present study, we address this limitation of seal resistance by combining physico-chemical and electrophysiological techniques with a global statistical design of experiments (DOE) approach in order to better evaluate and discriminate the vital factors required for the formation of seals. We previously achieved several gigaohm seal recordings with thermal oxide PECVD-coated devices but the majority of the seal resistances were below 200 MΩ [14], as also reported by other authors [9, 16, 17]. Here, we aim improving the mean seal resistances and the percentage of seal resistances higher than 200 MΩ since 200 MΩ

constitutes a reliable minimum threshold for reliable ion currents recordings. We also aim providing additional information about polar and dispersive contributions of surface energy, surface atomic composition and electrical capacitance. A DOE matrix was built with a combination of 5 parameters which lead to the study of 6 types of silicon chips. In this set of chips, 2 groups could be distinguished: chips with a Si_3N_4 LPCVD (Low Pressure Chemical Vapour Deposition) coating and chips with SiO_2 PECVD surface. Surface characterization, chemistry and topology, were carried out using XPS, AFM, ionic probes, surface energy, droplets angle measurements and impedance spectroscopy. In parallel, cell suspension protocols were optimized to preserve cell viability and minimize aggregates. In order to be consistent with traditional patch-clamp recordings, electrophysiological measurements of ion channel activity and dose-response curves of inhibitors were carried out on three cell lines (CHO and HEK293), both stably expressing various ion channels such as potassium channels (IRK1, hERG) and sodium channels ($hNa_v1.5$). These ion channels were chosen for their particular interest for pharmaceutical companies and for their specific biophysical properties (fast activation / inactivation kinetics).

2. Materials and methods

2.1. Cell preparation

Chinese hamster ovary (CHO) cells were chosen for the study of cell suspension quality. CHO cells were cultured in Ham's F12 medium supplemented with Glutamax (Gibco), 10% fetal calf serum (FCS) and 1% antibiotics. At 90% confluence, cells were rinsed twice in phosphate buffered saline (PBS) and then incubated 3-5 minutes at 37°C with either trypsin 25% (Gibco) or 0.3 ml of accutase (PAA Laboratories) in a 25 cm^3 flask. Trypsin was inhibited by adding culture medium containing FCS to the flask whereas accutase action was stopped by diluting the accutase solution ten-fold in PBS. Cells were centrifuged twice at 300

rpm for 5 minutes and resuspended in PBS. Cell viability was determined with the trypan blue exclusion assay. Enzymatic cell aggregates dissociation was carried out by incubating the cell suspension in 10% of accumax in PBS for 5 minutes. Cells were then centrifuged and resuspended. Mechanical cell aggregate removal was carried out by preparing a cell suspension in electrophysiological medium at 10^6 cells per ml and filtering it on a 40 µm mesh (Becton Dickinson). The percentage of aggregated cells was calculated using a counting Kovas slide (Dutcher). The cell preparation in 1 ml or 0.5 ml eppendorf tubes was placed on a carrousel for continuous mixing to limit cell aggregation. Viability and percentage of cell aggregation were monitored over time by taking samples at various time points over 4.5 hours. Human Embryonic Kidney 293 (HEK-293) cells were cultured in flasks in Dulbecco's modified Eagle's medium supplemented with 10% (v/v) FCS, 1.2 mg/ml geneticin, 1% penicillin-streptomycin and 1% L-glutamine.

2.2. Recombinant cell lines

Adherent CHO and HEK293 cells were chosen for their common use as expression systems of ion channels:

sCHO-IRK1: CHO-K1 cells were stably transfected with pcDNA3.1-HA-mIRK1 (Creacell, La Tronche, France), a plasmid carrying the coding sequence of the mouse IRK1 protein (or Kir 2.1) (NM_008425). Cells were cultured in Ham's F12 medium supplemented with 10% (V/V) foetal calf serum, geneticin (0.4 mg/ml), penicillin (50 U/ml), streptomycin (50 µg/ml) and L-glutamine (2 mM).

sHEK-hERG: The recombinant HEK293 cell line stably expressing the human ERG (ether-a-go-go related gene) potassium channel (NM_000238) was obtained from CreaCell. The cell line was cultured in Dulbecco's modified Eagle's medium supplemented with 10% (V/V)

FCS, geneticin (1.2 mg/ml), penicillin (50 U/ml), streptomycin (50 µg/ml) and L-glutamine (2 mM).

sHEK-αNav1.5 The recombinant HEK293 cell line stably expressing the alpha human Nav1.5 sodium channel subunit (NM_000335) was obtained from CreaCell. The cell line was cultured as described for the sHEK-hERG cell line.

2.3. Fabrication of Biochips

The process starts with 4 inches double-sided polished p-type (100) 450 µm thick silicon wafers. A thick silicon oxide is deposited using a TEOS (Tetraethyl orthosilicate) process on both sides of the wafer. For the KOH wet etching a silicon nitride mask is used. To do so, 1200 Å of LPCVD nitride and 1µm of amorphous silicon are deposited on both sides of the wafer. The layer of amorphous silicon is needed to etch the thick silica layer with the required accuracy. An array of nine circles with a pitch of 6 mm in the nitride layer on the amorphous silicon is created by mask contact lithography and plasma etching. A split is introduced in the batch in order to obtain chips with thin dielectric membrane (P1, P2 and P3 with 2 µm SiO_2 TEOS) and chips with high dielectric membrane (P4, P5 and P6 with 7 µm SiO_2 TEOS) on separate wafers. In order to protect the micrometric holes during KOH anisotropic etching, a metal protection made of 30 nm of Chromium and 200 nm of Gold is deposited. The patterns of the pyramids are transferred in the silicon nitride using standard contact lithography. Then the back side TEOS is plasma etched during approximately 9 hours. When pyramids are created, the front metal protections are etched by wet etching using KI/I2 and chrome etches. Mineral protections (Si_3N_4 and SiO_2) are dry etched using Reactive Ion Etching (RIE) techniques and micrometric holes are then “re-open”.

In order to minimize capacitances, the surfaces of the pyramids on the batch P2, P3, P4 and P5 chips were oxidized with a supplementary PECVD deposition of 1.5 µm maximum SiO_2 on the top, 1.5 µm on the back side and 0.7 µm on the inner walls (Figure 1A.).

2.4. A variance-based methodology for the study of silicon chips parameters

The device assembly were described previously [18]. Six types of chips were fabricated defined by 3 quantitative parameters: micropore diameter (D), dielectric surface roughness (R) and dielectric membrane thickness (T) and 2 qualitative parameters (hydrophilicity, -high or low- and material -SiO_2 or Si_3N_4). Statistical analyses were based on quantitative parameters. The ANOVA (ANalysis Of VAriance) analysis was chosen for this study with the use of a Fisher-Snedecor test ("F test") and was used to investigate the significance of the effects of the 3 variables D, R and T on the response function (i.e. the seal resistance value). The matrix is presented in Table 1A and Figure 1B. Approximately 20 samples were analysed in each group, a "sample" designing one microhole in a chip. Mean, standard deviation of each group and the coefficient of determination (R-squared) of the full correlation were calculated with the Design Expert v7.0 software. P values ≤ 0.05 for any factor indicated a significant effect of the corresponding variable on the response.

The study was carried out separately on chips with a Si_3N_4 LPCVD coating (chip types P1 and P6) and on chips with an additional SiO_2 PECVD layer (chip types P2, P3, P4 and P5) (Figure 1A&B). Chips were studied without (low hydrophilicity) and with (high hydrophilicity) O_2 plasma treatment, performed using a plasma oven (Plasma System Femto, Diener) at 100 W during 45 seconds.

Characterizations were conducted using SEM for microhole diameter and qualitative information about the microhole shape, AFM for the surface roughness, droplet angle measurements for hydrophilic quality of the surface as well as for dispersive and polar

contributions to surface energy, XPS for atomic links in the first 5 nm of the surface. The methodology is summarized in Table 1B and described hereunder.

Total chip capacitances were measured with a 263 A potentiostat and a 1025 frequency response detector (Princeton Applied Research, Oak Ridge, USA).

2.5. Characterization of silicon surfaces and geometries

Roughness determination

AFM experiments were performed with a DimensionTM 3100 AFM (Digital Instruments, Santa Barbara, CA) and a Nanoscope IV controller (Digital Instruments) equipped with a larger range scanner (maximum XY scan range of 90 µm x 90 µm with vertical Z range of 6 µm). Measurements were obtained in the AFM tapping mode as previously described [11]. The tips were supplied by Nanosensor (reference NCH 50, fo = 300 kHz; K = 40 N/m). The cantilever was made of silicon with an aluminium coating. Dimensions of the cantilever were as follows: thickness = 4 µm; length = 125 µm; width = 35 µm and the tip was characterized by a height of 10–15 µm, a tip radius of 10 nm and a half cone angle of less than 10°. All roughness values in this paper refer to the root-mean-square (rms) roughness of the height profile.

Quantitative chemical identification of surfaces species

Surface analyses were performed by X-ray photoelectron spectroscopy (XPS) at $8x10^{-9}$ mbar in an S-Probe spectrometer from Surface Science Instruments. Samples were irradiated with a monochromatic, micro-focused Al Kα source (1486.6 eV). The ejected electrons were collected at a take-off angle of 25° for enhanced surface sensitivity by an analyzer providing an energy resolution of 1.4 eV for survey spectra and 0.8 eV for the core level spectra. The energy scale was calibrated against the C 1s energy position of adventitious carbon C-C

measured on a metallic surface at 284.6 eV. The binding energy and intensity of the photoelectron peak determined the elemental identity, its chemical state and quantity. The mean analysed depth is about 5 nm.

Drop angle and surface energy measurements

Contact angles were measured on solid substrates at room temperature using the sessile drop method on the drop shape analysis system G10/ DSA10 (Krüss, Germany) with three different liquids (di-iodomethane, ethylene glycol and water). The average values of contact angles were determined from at least 4 droplets of each liquid. Surface energy fractions (disperse fraction and polar fraction (electrostatic fraction and hydrogen bridges)) of the substrates were determined using the extended Fowkes method [19].

2.6. Electrophysiology

Cells were pre-washed with PBS. On the basis of results (see below), trypsin was used to detach the cells and a cell suspension in electrophysiological medium was prepared at 10^6 cells per ml, filtered on a 40 µm mesh and kept on a carrousel before use.

Cell to chip resistance measurements (voltage response to current pulse) and ionic currents recordings were performed using our Multipatch-on-a-chip device previously described in [14, 18]. Experiments were conducted at room temperature (20°C) and cell currents were recorded in the whole-cell mode. For each experiment, a single micropore out of the nine present on each chip was used as follows: the bottom chamber of the device was first filled with the appropriate solution, followed by the upper chamber. Care was taken to eliminate bubbles in the fluidic circuit. Micropore resistance (Rh) was monitored by applying a square wave of voltage (5 mV amplitude and 10 ms duration) across the microfluidic chambers through the micropore with Ag/AgCl electrodes. The cellular suspension was then injected

into the upper chamber (~2500 cells/chamber) and a negative pressure of -20 to -50 mbar was applied to the lower chamber in order to attract one cell onto the micropore while simultaneously monitoring patch resistance. This phase of the process was successfully completed within 30 seconds. The negative pressure was maintained to promote contact between the cell membrane and micropore walls and released following the establishment of a high resistance seal. Whole-cell configuration was obtained by applying a 1 V pulse during 100 µs to snap the isolated membrane patch, and/or by applying a brief and strong suction. Subsequently, voltage control and current recordings from the cell membrane were performed. Acquisition was performed with the Multiclamp 700A amplifier (Axon Instruments, Union City, USA). All traces were sampled at 20 kHz and filtered at 2 kHz.

For the chip characterization, the seal success rate was based on acceptable seals higher than 200 MΩ, the minimal threshold needed to record ionic currents under the whole-cell configuration. Experimental conditions for these models were similar to those used in conventional patch-clamp experiments, where the “bath” solution becomes the upper chamber solution and the “intrapipette” solution the lower chamber solution.

For sCHO-IRK1 cells, the upper chamber solution contained (in mM): 118 NaCl, 5.6 KCl, 2.4 $CaCl_2$, 1.2 $MgCl_2$, 10 HEPES, 11 glucose, pH 7.4 (with NaOH), conductivity 1.32 S/m. In inhibition experiments, $BaCl_2$ (Sigma, St. Quentin Fallavier, France) was added. The lower chamber contained (in mM): 107 KCl, 1 $MgCl_2$, 2.5 Na_2-ATP, 10 EGTA, 10 HEPES, pH 7.4 (with KOH), conductivity 1.17 S/m. Current–voltage (I–V) relationships were obtained using voltage steps from 0 to −120 mV in 10 mV steps during 200 ms.

For sHEK-hERG cells, the upper chamber solution contained (in mM): 118 NaCl, 5.6 KCl, 2.4 $CaCl_2$, 1.2 $MgCl_2$, 10 HEPES, 11 glucose, pH 7.4 (with NaOH), conductivity 1.32 S/m at room temperature. In inhibition experiments, terfenadine (Sigma, St. Quentin Fallavier, France) was added. The lower chamber contained (in mM): 30 KCl, 110 K-

aspartate, 1 $MgCl_2$, 0.1 $CaCl_2$, 1 EGTA, 10 HEPES, pH 7.4 (with KOH), conductivity 1.30 S/m at 22°C. Current–voltage (I–V) relationships were obtained using a negative holding potential at -80 mV and a depolarisation step of 1 s at 60 mV followed by repolarization steps ranging from +40 to −100 mV in 10 mV steps during 3 seconds.

For sHEK-αhNav1.5, the upper chamber solution contained (in mM): 137 NaCl, 4 KCl, 5 $BaCl_2$, 1 $MgCl_2$, 10 HEPES, 10 glucose, pH 7.3 (with NaOH), conductivity 1.18 S/m at 19°C. In inhibition experiments, gonyautoxin (National Research Council Canada, NRCC) was added. The lower chamber contained (in mM): 135 CsF, 10 CsCl, 5 NaCl, 10 HEPES, 5 EGTA, pH 7.3 (with CsOH), conductivity 1.58 S/m at 22°C. Current–voltage (I–V) relationships were obtained using a negative holding potential at -100 mV followed by voltage steps from -90 to +60 mV in 10 mV steps during 20 ms and finally returning to a holding potential of -100 mV.

3. Results

3.1. Protocol for cell preparation

In order to minimize aggregates, kinetic curves of viability and aggregate formation were established for a panel of protocols used in cell detachment and resuspension. We compared trypsin *versus* accutase treatments as procedures to harvest cells. The choice of accutase, a formulated mixture of digestive enzymes, was motivated by previous results in cellular engineering [20, 21] since it was shown not to influence the cell current density [21].

Our results show that detachment of cells with trypsin gave higher cell viability than that with accutase (Table 2). On the downside, cell aggregation was also higher with the trypsin protocol. Removal of cell aggregates proved to be more efficient and cell friendly using a cell mesh rather than using accumax to dissociate the aggregates. After accumax treatment, viability dropped by 40-50% whereas the cell mesh decreased the cell suspension viability by

only 5%. Viability then remained stable with gentle mixing on a carousel for more than 4 hours. Thus, trypsin combined with filtering of the suspension over a cell mesh provided the best balance between viability and cell dispersion and this protocol was therefore used in all electrophysiological assays.

3.2. Effect of material and surface charges on cell sealing values

Chip parameters are summarized in Figure 1B. The seal resistance values and percentage of seals higher than 200 MΩ are shown in Figure 1C. Two groups of chips can be distinguished: those (P1, P5 and P6) providing a low percentage of acceptable seals (<50% of seals >200 MΩ) and those (P2, P3 and P4) providing a percentage higher than 60%. P1 and P6 were the only ones that had an additional Si_3N_4 coating at the surface of the chip. Thus, this coating does not seem to favour the cell sealing. The favourable effect of the type of material (SiO_2 versus Si_3N_4) on high resistive seal formation was confirmed by comparing P1 and P2 that only differed from their surface material (Figure 2B). This observation is less obvious between P5 and P6 (50 % seals > 200 MΩ), but the low rate of acceptable seals is likely due to the hole diameter as demonstrated below (Figure 1C).

The effect of surface charges on seal quality is presented in Figure 2. Our first observation was the noticeable improvement of seal quality with surface plasma O_2 treatment (Figure 2A). Without any treatment (n=27 µholes), the seal resistance remained lower than 100 MΩ and therefore did not allow ionic current recordings. With O_2 treatment performed on all types of chips (n=102 µholes), 67% of seals were higher than 200 MΩ and thus clearly appropriate for whole-cell recordings. Typical success rate of gigaseals (% of seals > GΩ) was 44% (Figure 2A) when performed on O_2 plasma treated SiO_2 chips while whole-cell recordings were subsequently obtained in around 40%. Generally, the recordings on this kind of chips were stable and lasted around 20 minutes.

Contact angles in Figure 2C reflect the hydrophilic properties of the studied surfaces. Figure 2C presents the values of water droplet angles obtained on 4 different surfaces. Each value is the mean of 5 measurements. For both surface coatings (SiO_2 and Si_3N_4), the O_2 plasma treatment drastically reduced the contact angles from 23 degrees to around 3 degrees. Moreover, after plasma O_2 treatment, SiO_2 was slightly more hydrophilic than Si_3N_4. Total surface energy was measured using the droplet angle method with two other liquids, (diiodométhane and ethylene glycol). Figure 2C shows that O_2 plasma treatment noticeably increased surface energies from 63 to 68 mN/m for SiO_2 and from 62.5 to 67 mN/m for Si_3N_4. Moreover, after O_2 plasma treatment, SiO_2 showed a significantly higher surface energy than Si_3N_4. Polar and dispersive contributions are displayed according to the Owens and Wendt model. O_2 plasma treatment slightly reduced dispersive energy contributions (Van der Waals forces) whereas it noticeably increased the polar interactions (hydrogen bonds and electrostatic interactions). Dispersive energy is higher on O_2 plasma treated SiO_2 surfaces than on O_2 plasma treated Si_3N_4 whereas polar energy variation is weak between both surfaces.

In XPS experiments, four kinds of surfaces were analyzed: SiO_2 and Si_3N_4 after deposition and cleaning by Caro process (H_2O_2/H_2SO_4), and the same samples after an additional O_2 plasma treatment (Figure 3). We used XPS to analyze the fine atomic composition of the top 5 nm layer of the surface. The survey spectra (Figure 3A) showed in all cases the presence of Si, O, C and N with various concentrations but without any others elements. The low quantity of C and O was consistent with usual environment contamination. Elementary compositions (Figure 3C) were determined using core level spectra performed on Si2p, O1s, N1s and C1s lines (Figure 3B).

SiO_2 samples: The Si/O ratio was close to that expected with SiO_2. A slight increase of the ratio was observed after O_2 plasma together with a very slight broadening of the Si2p line towards lower binding energies (Figure 3B). Nitrogen is detected inside the films, and is

involved simultaneously in both N-Si and H-Si bonds. After O_2 plasma treatment the nitrogen concentration decreased and the remaining nitrogen had only oxygen as neighbouring atoms.

Si_3N_4 samples: The Si/N ratio was higher than expected from the internal Si_3N_4 stoichiometry, and a large quantity of oxygen was included in the few nanometers which were analyzed. The Si2p line was broadened towards higher binding energies: the two Si-N and Si-O bonds were present and indicated the presence of SiO_2 on Si_3N_4 layers, SiO_2 becoming the main phase after O_2 plasma treatment, as observed in Figure 3B where the Si2p line was centred near the Si2p/SiO_2 one and broadened towards lower binding energies due to charge effects. The O1s spectra showed that binding energies for oxygen were the same for all surfaces, confirming the presence of SiO_2 on the surface of Si_3N_4 layers.

3.3. Effect of micropore diameter on cell sealing values

Micropore diameters were measured by SEM with a precision of 0.1 µm and are given in Figure 4. The micropore diameter and shape were previously demonstrated to influence the seal quality [14]. This was also observed here with P4 and P5 that only differ little in their micropore diameter. Figure 4 shows that decreasing the diameter (Ø) from 2.5 µm (P5) to 1.8 µm (P4) increases seal success rate (% of seals > 200 MΩ) from 50% to 66%. This difference based on the criterion "% of seals > 200 MΩ" is clearly noticeable (Figure 4, inset).

3.4. Effect of roughness and dielectric membrane thickness on cell sealing values

AFM scanning of the 6 different surfaces are presented in Figure 5A. 2 groups of roughness ranges can be distinguished. Lowest roughness's around 6 Å were obtained on surfaces that had no or very thin SiO_2 PECVD deposits (respectively P1 and P2 chip types). By contrast, chips with a thick SiO_2 PECVD deposit (at least 1 µm) showed a roughness around 50-55 Å (P3 to P6 chip types) indicating that the silicon oxide deposition had strongly altered the

surface topology, as previously described [13, 14]. For the surface roughness and the dielectric membrane thickness, the technological process was not able to completely differentiate both parameters. Nevertheless roughness and dielectric membrane thickness do not seem to alter the seal quality as shown in Figure 5B. P4 devices with the highest aperture depth (8.62 µm) and the highest roughness (55 Å) produced 66% of seals higher than 200 MΩ whereas P2 devices with the lowest aperture depth (2 µm) and the lowest roughness (5 Å) produced 63% of seals higher than 200 MΩ. Similarly, the difference in aperture depth was weak between P2 and P3 whereas the difference in surface roughness was high. Even so percentages of good seal yield were similar.

The thickness of the dielectrical membrane influences the total capacitance of the chips. Total capacitance of our chips and cell-patch site resistance were modelled as previously described [14]. As illustrated in Figures 6A&B the global capacitance remains equivalent to the capacitance C2 with the hypothesis that C5 is much higher than C3 and C4. The capacitance study was performed on P1, P3 and P4 chip types constituted with different layers of dielectric materials (Figure 6C). Capacitance measurements were performed using smaller o-rings (1.4 mm inner diameter) than in previous studies (3 mm inner diameter) to reduce the fluid contact surface from 11.3 mm² [14] to 4.4 mm². Results of P3 compared to those of P1 show that an additional SiO_2 PECVD layer of 1.5 µm reduced the capacitance from around 100 pF to around 50 pF by increasing the thickness of the SiO_2 layer on the pyramids surface by 0.7 µm (LETI background). Moreover P4 chips show that an additional SiO_2 PECVD layer of 1.5 µm added to a higher thickness of SiO_2 TEOS reduced the capacitance to around 30 pF. Because capacitance is an important factor to measure ionic currents with fast kinetic, P4 chips, presenting the lowest capacitance, were chosen to perform the electrophysiological validation (Figure 7).

3.5. Electrophysiological validation

Providing 66% of seals higher than 200 MΩ and the lowest capacitance, P4 chips were evaluated for electrophysiological validation and pharmacological testing on 3 cell lines stably expressing various potassium and sodium ion channels. Moreover, our experiments have shown that P4 provided the most stable seals for sHEK-hERG channel recordings (data not shown). Representative current traces can be seen in Figure 7A, showing the current-voltage relationship of potassium channels stably expressed in HEK293 cells. Terfenadine, a well characterized inhibitor of hERG channel was selected to obtain dose-dependently inhibit hERG currents. The IC_{50} of 13 ± 4 nM (i.e. the concentration of drug required to inhibit 50% of the current) was in the range of the values found with other patch-clamp devices, although a severe discrepancy can be observed in the literature concerning this IC_{50} value with automatic patch-clamp systems [22, 23]. In the present study, the recordings on P4 chips, with HEK293 cells, were stable for 20 min so that entire dose-response curves could be extracted from single cells.

As a second validation test, whole cell K^+ currents recorded from sCHO/IRK1 channels with P4 chips are presented in Figure 7B. Characteristic inward rectifying potassium currents could be elicited with a very low seal leak, as compared with our previous work [14], illustrating the good performance of P4 chips. The recordings were stable (> 20 min) so that entire dose-response curves could be extracted from single cells. The IC_{50} of the unspecific Ba^{2+} divalent blocker was close to 85 µM, a value that is in agreement with other published observations.

As a third test, whole cell Na^+ currents recorded from sHEK/αNav1.5 cells channels with P4 chips are presented in Figure 7C. α$hNa_v1.5$ ion channels rapidly (0.8 ms) activate and inactivate in response to voltage changes (arrow in Figure 7C). In order to validate the electrical signature of the channel, gonyautoxin, a specific toxin inhibitor, was dispensed. As

expected, a complete whole-cell sHEK-αhNa$_v$1.5 current inhibition was obtained with 10 nM gonyautoxine whereas the IC_{50} of gonyautoxin was found to be close to 7 nM as determined by conventional patch-clamp in our lab (consistent with values from the literature; not shown).

3.6. Variance analysis

Variance analyses were performed either with the 3 variables, D, R and T (multi-linear model) or with only one parameter (D) (simple linear model) (Table 1A).

Multi-linear model: variance analysis was performed with the 3 variables, D, R and T. The calculated F-value was 1.26 implying the model was not significant over noise. There was a 29% (P-value = 0.2922) chance that a « model F-value » this large could occur due to noise. Values of P-value less than 0.1000 indicate model terms are significant. In the present case, there were no significant model terms. Nevertheless, the analysis showed that there was a 78.6% chance that the effect of factor D (Diameter) on the response (seal resistance value) might be significant (see the simple linear model). The final equation in the multi-linear model was: Seal Resistance (MΩ) =1269 – 323 D – 11 T + 1.08 R.

Simple linear model: variance analysis was performed only with D variable. In this second case, the F-value of 3.8 implied the model to be significant but with 5.4% chance that a « Model F-value » this large could occur due to noise. In the present case, **D** was a significant model term with a P-value of 0.05. The final equation was: Seal Resistance (MΩ) =1321 - 362 D.

4. Discussion

Planar substrates have characteristics and constrains that differ from those of glass micropipettes. To apprehend these characteristics, a multi-scale surface characterization

(using XPS, AFM, surface energies determination, etc) is an asset when defining important seal parameters that discriminate planar patch-clamp from traditional patch-clamp. On the basis of quantitative data describing physicochemical chip properties, our study demonstrates that two parameters are crucial in determining seal quality: nature of surface energy and micropore diameter.

Our first observation was the noticeable improvement of seal quality with surface plasma O_2 treatment. Such an improved seal quality and stability was expected since hydrophilic surfaces had been previously shown to promote the attachment of hydrophilic cell membranes [14, 24]. Moreover O_2 plasma treated SiO_2 is more favourable to high resistive seal formation than O_2 plasma treated Si_3N_4 providing higher surface and higher dispersive energies than Si_3N_4. Therefore the discrepancy in the seal quality seems to be more related to a discrepancy in dispersive than in polar energies. Corey and Stevens had hypothesized in 1983 [24] that four sources of interaction could participate in the glass-membrane seal: ionic bonds, hydrogen bonds, divalent ions forming salt bridges and van der Waals' forces, without giving a precise order of importance. The authors presumed that bridges, hydrogen bonds and van der Waal's forces were especially important. Since then, no study had demonstrated experimentally the influence of dispersive interactions in the seal process. Compared to [16] where authors have only considered contact angles as surface energy parameters, in our study, drop angle and surface energy measurements discriminate dispersive (van der Waals) and polar (electrostatic and hydrogen bonds) energies. Our results demonstrate that dispersive energy more than polar energy has a high impact on seal quality, consistent with a recent study that stipulates that the primary attractive force for the gigaseal seems to be van der Waals attraction, the same forces that account for the tape adhesion [25]. Van der Waals interactions are not chemically specific force and apply to glass (silicate), proteins, polysaccharides and lipids. The positive impact of dispersive interactions is observed while

no change in atomic composition occurs as it is demonstrated by XPS. These results confirm that the seal quality is related to surface charges and not to the surface atomic composition since after O_2 plasma treatment, SiO_2 and Si_3N_4 provide the same materials.

Another parameter we are able to control as a function of TEOS SiO_2 layer and PECVD deposits is the microaperture size. The results obtained from the analysis of multi-linear model and simple linear model show that the influence of micropore diameter on seal quality depends on whether the parameter is considered alone or as a group with other parameters. Statistical analyses concerning the relationship between mean resistance of the seal and pore diameter show that the effect of diameter on seal resistance value exists; nevertheless it is not very significant (P=0.05). The fact that this rather moderate effect is significant in the simple linear model is due to the large number (n=102) of trials and is probably underestimated due to the wide dispersion of the results, as it is often observed in planar patch-clamp [16]. In this manuscript, we recorded voltage-dependent Na^+ current with typical biophysical characteristics and illustrated its inhibition by gonyautoxin with seal resistance around 300 MΩ (Fig. 7C). This result validates the criterion chosen of "percentage of seals higher than 200 MΩ". If we consider this criterion, a large difference is observed between 1.8 µm (P4) and 2.5 µm (P5) since this increase from 50% to 66% represents a 32% increase in “acceptable seal” probability.

By contrast to micropore diameter and dispersive energy, roughness and membrane thickness do not significantly influence seal quality. This result was quite surprising since a significant effect of membrane thickness was expected. It was indeed previously observed that the seal quality depends on the length of membrane invagination into the micropore and the total surface contact [26]. Experimental observations were published showing for example the 3.3 µm invagination of a fluorescent cell membrane in a 2 µm sized channel [27]. Such studies emphasize a mechanical role of the invagination that obstructs the microaperture and the

important role of a sufficient contact area between the membrane and the wall of the pore. Theoretical models have shown that in a gigaseal the distance between cell membrane and planar surface is of atomic-scale (around the Angstrom, [28]), which excludes adherent proteins in this sealing process. Another group has modelled a cell spread on the pore of a fibronectin-coated surface [29] and have confirmed that extracellular matrix hampers the formation of a resistive seal. Therefore, we expected to observe a mechanical positive effect of membrane invagination on the seal quality by increasing the aperture depth. In our case, a high membrane depth does not hamper nor does it increase seal formation. In our conditions, due to technological process constraints, membrane thickness and surface roughness parameters are not completely independent and consequently the estimations of the parameters in the multi-linear model are not statistically independent. We previously reported higher seal resistances with PECVD (1 µm deposit at the top of the surface) compared to thermal oxide surfaces, whereas PECVD treatment increased surface roughness [14]. Our methodology probably underestimates the real effect of membrane thickness that remains here slightly correlated to surface roughness. Nevertheless, the comparisons between P4 and P2 (both chips presenting opposite characteristics in terms of roughness and aperture depth), show that both parameters have a low impact on the seal quality. In other words a high membrane thickness and a high roughness don't significantly hamper the sealing process in our conditions. It appears that, taken together, both parameters compensate their own effects, since a high membrane thickness has been shown to be favourable to seal quality, whereas a high roughness has been reported to hamper seal formation [16]. Nevertheless, as mentioned by [16], it is possible that increasing surface roughness into the nanometer range where protein adsorption and denaturation occur [30] could facilitate seal formation. Further refined investigation is probably required to reliably ponder each parameter and thus to better understand independent effects. One solution would be to perform Deep UV lithography

instead of mask contact lithography in order to directly process micron-sized hole with high aspect ratios allowing limiting the PECVD deposit.

In our study, P4 chips afforded the 'best' properties among P1-P6 types with the smallest aperture diameter (1.8 µm), the highest aperture depth (8.62 µm) and the lowest capacitance of 29 pF. By contrast to [16], we think that a too high aperture length (of 30 µm as suggested by authors) may not be an advantageous design change since it may provide limitations in the suction process as we indeed observed, and thus may limit the probability to obtain a successful whole-cell configuration. We also consider as relevant the h/∅ ratio as a critical parameter for seal formation and quality (stability). In our study, P4 chips produce the highest h/∅ ratio around 4.8 compared to P1 (1.11), P2 (1.23), P3 (2.18), P5 (3.45) and P6 (3.63). This high ratio seems to be a favourable parameter well suited for both HEK293 cells (15 µm diameter) as well as CHO cells (20 µm diameter) electrophysiological analyses. As for the high roughness of the P4 chips, it does not seem to hamper seal formation as suggested before [14] or its potential negative impact is here compensated by the positive impact of a high h/∅ ratio.

P4 provided suitable results in terms of seal quality with a high mean seal resistance around 600 MΩ, which is far much higher than the one reported in recent studies [16], and also provided a higher yield of successful seals around 70%. For electrophysiological validation, P4 were used for making dose-response curves with drugs or non-specific inhibitors. As compared to previous results with IRK1 channels (only 16% success rate in forming seals higher than 1 GΩ, [14]), the seal resistance is here increased (70% of seals higher than 200 MΩ and 40% gigaseals) and therefore the quality of recordings is optimized with no current leak. Such chips provided sufficiently stable seals allowing pharmacological studies since IC_{50} values were determined in both cases with 4 concentrations of channel blocker on a single cell. The improved success rate reported here may have been influenced

by the reduced capacitance and also by a higher h/∅ ratio (8.62 µm) compared to our previous study (3.62 µm) [14]. This change represents a 300% increase in aperture depth for our devices. This factor may have significantly contributed to the improved success rate reported in this study optimizing the probability of successful gigaohm seal formation and the maximum obtainable seal resistances.

As reminded by [31], any silicon-based strategy for making a patch partition has to tackle the problem of large capacitances. In our study, the original superposing of dielectric layers, both on the planar surface and on the inner walls of the chips, reduced the capacitance from 100 pF to around 30 pF. Specific determination of capacitances from each dielectric layer should allow discriminating which layer has a major influence on the global capacitance. The global capacitance of the chips remained equivalent to C2 that is to say to the TEOS SiO_2 upper layer capacitance. We previously investigated the effect of chip passivation on typical electrical characteristics of chips [14]. It was shown that a 3.62 µm thick silica membrane, obtained following a 1.5 µm PECVD SiO_2 layer deposition, provided a capacitance of about 50 pF. As expected, we could here further reduce the capacitance (from 50 pF to 30 pF) by increasing the insulator TEOS layer, by an additional SiO_2 PECVD layer and by reducing the fluid contact surface. Since our membrane is SiO_2-made, our microfabrication process allowed the design of a thicker TEOS SiO_2 membrane, a feature more difficult to obtain with silicon bulk-made membranes [9]. The value of 30 pF is in the best range of those already published for silicon chips [32], except for silicon-on-insulator (SOI) substrate that provides lower noise current [33]. Our low capacitance allowed us to measure efficiently Na^+ current, known to present very fast activation kinetics (0.8 ms). The subsequent high roughness of the surface (>10 Å) does apparently not hampered good seals rates, as previously observed [14]. Taken together, our previous results [14] were the building blocks of the present systematic study that provides additional and refined information in

terms of surface energy, dispersive interactions, hydrophilicity, atomic composition and dielectric material.

Our work aims to propose a multi-scale approach allowing testing a panel of different kind of chips, and finally to discriminate parameters that are able to suite specific requirements of different cellular preparations. Therefore, the good quality of cell isolation (correct cell density, good morphology, few aggregates and dead cells, etc…) is also of great importance for the seal quality and stability. Since a cell is caught blindly from a cell suspension, most cells must be healthy and the amount of aggregates very low since cell clusters are detrimental for the success rate of automated gigaseal formation [31]. Unless a cell line is grown in suspension, cells need to be acutely dissociated and the cell isolation procedure becomes a critical step for the seal formation. As reminded by [15], the cytoskeleton of a cell redistributes after it has detached from the culture dish. These mechanical properties probably explain the distinct ability of seal formation from adherent and non adherent cells. Because no specific detaching agent has been really discriminated in literature, we aimed to define our own biological protocol for cell preparation. Here the cell suspension optimization was studied before the chip study since introducing non-viable cells and cell aggregates in our assays would have hampered the results of chip parameter analyses. Finally, we want to point out that our procedure, leading to a good compromise between viability and aggregates, will not systematically translate to other cell lines that differ from their membrane composition. Indeed, cell preparation procedures often need some adjustments for each new cell model [15].

Functional high throughput screening technologies have enabled to increase the number of assays on ion channels, now fully exploited as drug targets [19, 20, 27]. The planar patch-clamp principle is at present used mainly for automated and parallelized whole-cell patch-clamp recordings as evidenced by a considerable number of publications from academic

[9,12,14,15,27,33,34-37] as well as industrial applications [1,38]. Besides scaling-up the recordings, being able to design and manufacture specific low capacitive chips for example, only by modifying a defined parameter, could be useful for such applications as drug screening. P4 chips afforded good electrophysiological validation both on sHEK-hERG and sHEK-hNa_v1.5 ion channels. In addition to hERG channels, hNa_v1.5 channels are challenging drug targets to early detect adverse side effects and are therefore important for *in vitro* cardiotoxicity assessment [23]. In this case, low capacitive chips are suitable for such channels (hNa_v1.5) with rapid activation and inactivation kinetics requiring exquisite voltage control to avoid artefacts. Because activation time constants are typically in the order of 0.5-1 ms, capacitive currents can obscure the peak current and should be compensated properly. This is illustrated in our study on stable cell lines expressing hNa_v1.5 channels (alpha subunit) but can be extended to other types of channels with fast kinetics.

5. Conclusion

The combination of a multiparametric physico-chemical characterization of surfaces with a statistical design approach provides a versatile strategy to enhance the performances of patch-clamp chips with regard to seal resistance and yield. More fundamentally, such a global systematic study provides new tools to gain insights into the physico-chemical basis of cell interaction during the sealing process. With our approach, two criteria (microhole diameter and dispersive energy) emerged as important for classifying chips as good or bad candidates for patch clamping applications. Investigating each parameter in a global way should help guiding the fabrication process and implementing active functions on chips (recording electrodes, cell positioning process…). At the end, for a specific material (silicon for example), our approach provides a mean to standardize the fabrication process of consumables (chips) and therefore to increase the reliability and the reproducibility of the

seal. These findings may direct strategies for selecting appropriate surface topology and materials dedicated to biochips. Research on cell-to-chip interface is essential for defining conditions that improve the sealing process and may have more general implications in the field of cell adhesion on biomaterials. This study, which deals with material surface properties, should thus open new strategies in biochips development.

Acknowledgements

We thank Olivier Renault, from CEA Leti, for XPS analysis and graphical interpretation, Alexandra Fuchs from CEA DSV and Pierre-Yves Perche from Creacell, Grenoble for helpful discussions.

References

[1] Dunlop J, Bowlby M, Peri R, Vasilyev D, Arias R. High-throughput electrophysiology: an emerging paradigm for ion-channel screening and physiology. Nat Rev Drug Discov 2008;7:358-368.

[2] Gidrol X, Fouque B, Ghenim L, Haguet V, Picollet-D'hahan N, Schaack B. 2D and 3D cell microarrays in pharmacology. Curr Opin Pharmacol 2009;9:1-5.

[3] Curtis A, Wilkinson C. Topographical control of cells. Biomaterials 1997;18:1573-1583.

[4] Kane RS, Takayama S, Ostuni E, Ingber DE, Whitesides GM. Patterning proteins and cells using soft lithography. Biomaterials 1999;20:2363-2376.

[5] Mann BK, Tsai AT, Scott-Burden T, West JL. Modification of surfaces with cell adhesion peptides alters extracellular matrix deposition. Biomaterials 1999;20:2281-2286.

[6] Behrends J, Fertig N. Planar Patch Clamping. In: Neuromethods. W. Walz ed. Totowa, NJ: Humana Press Inc; 2007. p. 411-433.

[7] Terstappen G. Ion channel screening technologies today. Drug Discov Today 2005;2:133-140.

[8] Stett A, Bucher V, Burkhardt C, Weber U, Nisch W. Patch-clamping of primary cardiac cells with micro-openings in polyimide films. Med Biol Eng Comput 2003;41:233-240.

[9] Pantoja R, Nagarah JM, Starace DM, Melosh NA, Blunck R, Bezanilla F, et al. Silicon chip-based patch-clamp electrodes integrated with PDMS microfluidics. Biosens Bioelectron 2004;20:509-517.

[10] Dale TJ, Townsend C, Hollands EC, Trezise DJ. Population patch clamp electrophysiology: a breakthrough technology for ion channel screening. Mol Biosyst 2007;3:714-722.

[11] Sigworth FJ, Klemic KG. Patch clamp on a chip. Biophys J 2002;82:2831-2832.

[12] Klemic KG, Klemic JF, Reed MA, Sigworth FJ. Micromolded PDMS planar electrode allows patch clamp electrical recordings from cells. Biosens Bioelectron 2002;17:597-604.

[13] Sordel T, Kermarec-Marcel F, Garnier-Raveaud S, Glade N, Sauter-Starace F, Pudda C, et al. Influence of glass and polymer coatings on CHO cell morphology and adhesion. Biomaterials 2007;28:1572-1584.

[14] Sordel T, Garnier-Raveaud S, Sauter F, Pudda C, Marcel F, De Waard M, et al. Hourglass SiO_2 coating increases the performance of planar patch-clamp. J Biotechnol 2006;125:142-154.

[15] Chen CY, Tu TY, Chen CH, Jong DS, Wo AM. Patch clamping on plane glass-fabrication of hourglass aperture and high-yield ion channel recording. Lab Chip 2009;9:2370-2380.

[16] Curtis JC, Baldwin K, Dworak BJ, Stevenson JTM, Delivopoulos E, McLeod NK, Murray AF. Seal formation in silicon planar patch-clamp microstructures. J Microelectromech S 2008;17:974-982.

[17] Matthews B and Judy JW. Design and fabrication of a micromachined planar patchclamp substrate with integrated microfluidics for single-cell measurements. J Microelectromech S 2006;15:214-222.

[18] Picollet-D'hahan N, Sordel T, Garnier-Raveaud S, Sauter F, Ricoul F, Pudda C, et al. A silicon-based Multipatch device for ion channel current sensing. Sens Lett 2004;2:1-4.

[19] Chen Jie-Rong W. Studies of the surface free energy and surface structure of PRFE film treated with low temperature plasma. J Applied Polym Sci 1997;63:1733-1739.

[20] Weikert C, Eppenberger-Eberhardt M, Eppenberger HM. Cellular engineering of ventricular adult rat cardiomyocytes. Cardiovasc Res 2003;59:874-882.

[21] Tao H, Santa Ana D, Guia A, Huang M, Ligutti J, Walker G, et al. Automated tight seal electrophysiology for assessing the potential hERG liability of pharmaceutical compounds. Assay Drug Dev Technol 2004;2:497-506.

[22] Guo L, Guthrie H. Automated electrophysiology in the preclinical evaluation of drugs for potential QT prolongation. J Pharmacol Toxicol 2005;52:123-135.

[23] Brown AM. High throughput functional screening of an ion channel library for drug safety and efficacy. Eur Biophys J 2009;38:273-278

[24] Corey D, Stevens C. Science and technology of patch-recording electrodes. In: Neher BSaE, editor. Single-channel recording. New York: Plenum Publishing Corp.; 1983. p. 53-68.

[25] Suchyna TM, Markin VS, Sachs F. Biophysics and structure of the patch and the gigaseal. Biophys J 2009;97:738-747.

[26] Hamill OP, Marty A, Neher E, Sakmann B, Sigworth FJ. Improved patch-clamp techniques for high-resolution current recording from cells and cell-free membrane patches. Pflugers Arch 1981;391:85-100.

[27] Ionescu-Zanetti C, Shaw RM, Seo J, Jan YN, Jan LY, Lee LP. Mammalian electrophysiology on a microfluidic platform. P Natl Acad Sci USA 2005;102:9112-117.

[28] Diaz-Rivera RE, Rubinsky B. Electrical and thermal characterization of nanochannels between a cell and a silicon based micro-pore. Biomed Microdevices 2006;8:25-34.

[29] Urisu T, Asano T, Zhang Z, Uno H, Tero R, Junkyu H, et al. Incubation type Si-based planar ion channel biosensor. Anal Bioanal Chem 2008;391:2703-2709.

[30] Muller B, Riedel M, michel R, De Paul SM, Hofer R, Heger D, Grutzmacher D. Impact of nanometer-scale roughness on contact-angle hysteresis and globulin adsorption. J Vac Sci technol B 2001;19:1715-1720.

[31] Behrends JC and Fertig N. Planar patch clamping. In Patch-Clamp Analysis : advanced techniques, second ed, W.Walz (Ed), humana press; 2007. p. 411-433.

[32] Schroeder K, Neagle B, Trezise DJ, Worley J. Ionworks HT: a new high-throughput electrophysiology measurement platform. J Biomol Screen 2003;8:50-64.

[33] Zhang Z, Asano T, Uno H, Tero R, Suzui M, nakao S, et al. Fabrication of Si-based planar type patch clamp biosensor using silicon on insulate substrate. Thin Solid Films 2008;516:2813-2815.

[34] Brueggemann A, George M, Klau M, Beckler M, Steindl J, Behrends JC, et al. Ion channel drug discovery and research: the automated Nano-Patch-Clamp technology. Curr Drug Discov Technol 2004;1:91-96.

[35] Bruggemann A, Stoelzle S, George M, Behrends JC, Fertig N. Microchip technology for automated and parallel patch-clamp recording. Small 2006;2:840-846.

[36] Fertig N, George M, Klau M, Meyer C, Tilke A, Sobotta C, et al. Microstructured apertures in planar glass substrates for ion channel research. Receptor Channel 2003;9:29-40.

[37] Asmild M, Oswald N, Krzywkowski K, Friis S, Jacobsen R, Reuter D, et al. Upscaling and automation of electrophysiology: toward high throughput screening in ion channel drug discovery. Receptor Channel 2003;9:49-58.

[38] Priest BT, Swensen AM, McManus OB. Automated electrophysiology in drug discovery. Curr Pharm Design 2007;13:2325-2337.

Figure captions and tables

Figure 1.**Chips design for the multi-parametric study of the seal quality**.

A. Schematic cross-section of the chips dedicated for the Design of Experiment approach. 2 groups of chips are studied: one with a Si_3N_4 LPCVD surface (left) and the second one with an additional SiO_2 PECVD layer (right). *eSi_3N_4=1200 Å; eTEOS= 2 µm for P1, P2 and P3 or 7 µm for P4, P5 and P6. 0.1µm < ePECVD < 1.5 µm; 1.8 µm<Ømicropore < 2.5 µm; h=eSi_3N_4 + eTEOS + ePECVD; 2.12 µm < h < 8.72 µm.* TEOS: Tetraethyl orthosilicate; LPCVD: Low Pressure Chemical Vapour Deposition, PECVD: Plasma Enhanced Chemical Vapour Deposition.

B. Characteristics of the 6 microfabricated chips, studied according to 5 parameters. The high hydrophilicity is obtained with O_2 plasma treatment and low hydrophilicity is obtained without any treatment.

C. Seal resistance data for planar patch-clamp devices. The table shows the mean seal resistance along with the associated n number and standard deviation for the 6 different device groups. In addition the percentage of seals higher than 200 MΩ obtained for that group of devices is shown.

Figure 2. Effect of material and surface charges on seal resistance values and success rate.

A. Effect of the surface hydrophily (without or with O_2 plasma treatment) on the seal yield (in %) for all the chip devices (n=102 microholes).

B. Effect of the surface material (P1, Si_3N_4) and (P2, SiO_2) after O_2 plasma treatment on the seal resistance values (in MΩ) and on % of accepted seals (ie: % of seals > 200 MΩ) (inset).

C. Drop angle and surface energy (top). Dispersive energy (bottom, left) and polar energy (bottom, right) are displayed for both groups of chips (SiO_2 or Si_3N_4), without and with O_2 plasma treatment (+ Pl O_2).

Figure 3. Surface analyses using X-ray Photoelectron Spectroscopy (XPS).

A. Survey spectra of SiO_2 and Si_3N_4 after deposition and cleaning by Caro process (H_2O_2 /H_2SO_4), and the same samples after an O_2 plasma treatment. Spectra show in all cases the presence of Si, O, C and N without any others elements.

B. High resolution core level Si2p, C1s, N1s, and O1s photoelectron spectra (circles in A) of SiO_2 and Si_3N_4 after cleaning by Caro process, and the same samples after an O_2 plasma treatment. The scales of the intensities (counts) are different from the various samples and are adjusted to the maximum (see the Table C for a comparison of the intensities).

C. Quantitative XPS analyses: atomic concentrations determined on high resolution spectra from integral intensities of core levels onto Si2p, O1s, N1s and C1s lines. From binding energy and intensity of a photoelectron peak (in A.), the elemental identity, chemical state and quantity (%) of an element are determined.

Figure 4. Influence of aperture diameter on seal quality.

Effect of the µhole diameter (1.8 µm, P4 or 2.5 µm, P5) on the mean resistances values and on the % of accepted seals (ie: % of seals > 200 MΩ) (inset). * Significant difference between P4 and P5, P=0.05.

Figure 5. Effect of surface roughness and dielectric thickness on mean seal resistances and on seal yield.

A. Surface roughness determination on the 6 types of chips.

2 groups are distinguished : chips P1 and P2, with either no additional PECVD SiO_2 deposit (P1) or a low deposit (0.1 µm) (P2) present a low roughness around 6 Å and chips from P3 to P6, with a high PECVD SiO_2 deposit (1 µm) present a high roughness around 50 Å.

All roughness values refer to the root-mean-square (rms) roughness of the height profile. For each group of chips, R (rms) was determined on 3 chips, on a 1x1 µm² area, using the WSxM software.

B. Effect of the membrane thickness (2 µm, P2; 3.8 µm, P3 or 8.6 µm, P4) on the % of accepted seals (ie: % of seals > 200 MΩ) (inset).

Figure 6. Chip capacitance analysis and modeling

A. Cross section of the chip structure (P1 as for example) with a representation of all the capacitances (C_x) from the different dielectric layers. Each capacitance is characterized by a thickness (e) and a dielectric permittivity (ε) : $eSiO_2$=2µm, eSi_3N_4=0.12µm, $e_{native}SiO_2$=20A, εSiO_2=4.5, εSi_3N_4=7. Not drawn to scale.

B. A simplified model of the equivalent capacitance of the chip. The global capacitance corresponds to C2, « owing » that C5>>C3 and C5>>C2 (see text). C1, C4 and C2, C3 are measured with o-rings of 1.4 mm inner diameter. The C5 capacitance (14 nF) was considered since it represents a thin layer of oxide on the inner walls of the humid etching (10-20Å). The very low C6 and C7 capacitances are considered as negligible. With silicon viewed as a perfect conductor material and the resistance between C2, C3 and C5 as negligible, the 3 capacitances C2, C3 and C5 form a unique electrical node.

C. Effect of the dielectric membrane thickness on the chip capacitance.

“Theoretical” capacitances were measured according to B. “Measured” capacitances were measured with impedance spectroscopy. “Corrected” capacitances were obtained after subtraction of capacitance providing from the system assembly and electrical connectors (5 pF). A good correlation between corrected capacitances and theoretical ones is observed.

Figure 7. Electrophysiological validation of P4 silicon chips with IRK1, hERG and hNav1.5 ionic channels.

Whole-cell currents were recorded from potassium and sodium channels with P4 chips

A. Current recordings were performed from HEK cells stably expressing hERG channels. Current curve as a function of time (I=f(t)) was obtained using a negative holding potential at -80 mV then a depolarisation step of 1s at 60 mV then some repolarization steps +40 to −100 mV in 10 mV steps during 3 s (left with protocol upper side). Seal resistance was 1 GΩ. Current inhibition is displayed for 4 concentrations of Terfenadine (0.1 nM, 1 nM, 10 nM and 100 nM). For each concentration, 3 cells are tested. Note that all the concentrations are dispensed on the same cell that remains mechanically stable once the seal was established. Dose/response curve with Terfenadine (right) established from I =f(t). Terfenadine IC_{50} is thus determined on single cells with a good accordance with published data.

B. Inward rectifying potassium currents from CHO cells stably expressing IRK1 channels were elicited with activating voltage steps from 0 to −120 mV with 10 mV decrements (left). Seal resistance was 1 GΩ. Blocking effect is demonstrated on inward K^+ currents by the unspecific Ba^{2+} divalent (1 mM) (middle). Typical data are displayed without applying leak subtraction. Current–voltage relationship curves were obtained from previous current traces (no leak compensation). Dose-response curve (right) was determined with increasing concentration of $BaCl_2$. The IC50 value was in accordance with published data.

C. Current recordings were performed from HEK cells stably expressing hNav1.5 channels. Current curve as a function of time was obtained using a negative holding potential at -90 mV then some voltage steps from -60 to +30mV in 10mV steps during 20 ms then return to holding potential of -90 mV (left). Seal resistance was 300 MΩ. The arrow points out the current trace corresponding to -30 mV test potential. Currents activate and inactivate in 0.8 ms in response to voltage changes. The characteristic I/V curve (right) was investigated, without (filled circles) and with (open squares) Gonyautoxin inhibitor (10nM). Note that an IC_{50} of 7 nM was determined with conventional patch-clamp (not shown).

Table 1. Methodology of experiments.

A. The level of variables in statistical experimental design.

B. List of methods employed either to control the chip features once manufactured or to gain insights in the seal formation process.

Table 2. Study of the cell isolation procedure.

Viability kinetic study (up) and aggregates determination (bottom) with different protocols for cell preparation and conservation. Viability percentage is determined with 5 % variability, depending of the counting manual mode.

Figure 1

A.

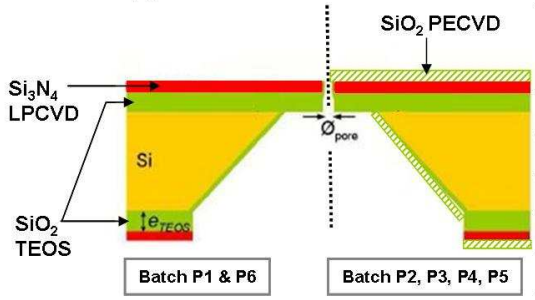

C.

Device type	n	Mean seal R (MΩ)	Stand Dev.	Seal > 200 MΩ (%)	Max seal R (GΩ)
P1	18	529	148	45	1.6
P2	16	791	168	63	1.6
P3	16	704	146	70	1.5
P4	15	626	158	66	1.5
P5	16	444	140	50	1.4
P6	17	440	105	50	1.4

B.

Chip / Parameter	P1	P2	P3	P4	P5	P6
$\varnothing_{pore}$ (µm)	1.9 ± 0.1	1.8 ± 0.1	1.75 ± 0.1	1.8 ± 0.1	2.5 ± 0.1	2.4 ± 0.1
h (µm)	2.12	2.22	3.82	8.62	8.62	8.72
Surface	Si_3N_4	SiO_2	SiO_2	SiO_2	SiO_2	Si_3N_4
Roughness (Å)	5.9 ± 2.1	6.2 ± 1.3	49.6 ± 5.3	54.0 ± 3.2	54.6 ± 2.8	56.1 ± 3.8
Hydrophily (High/Low)	High + Low	High + Low	High + Low	High + Low	High + Low	High + Low

Figure 2

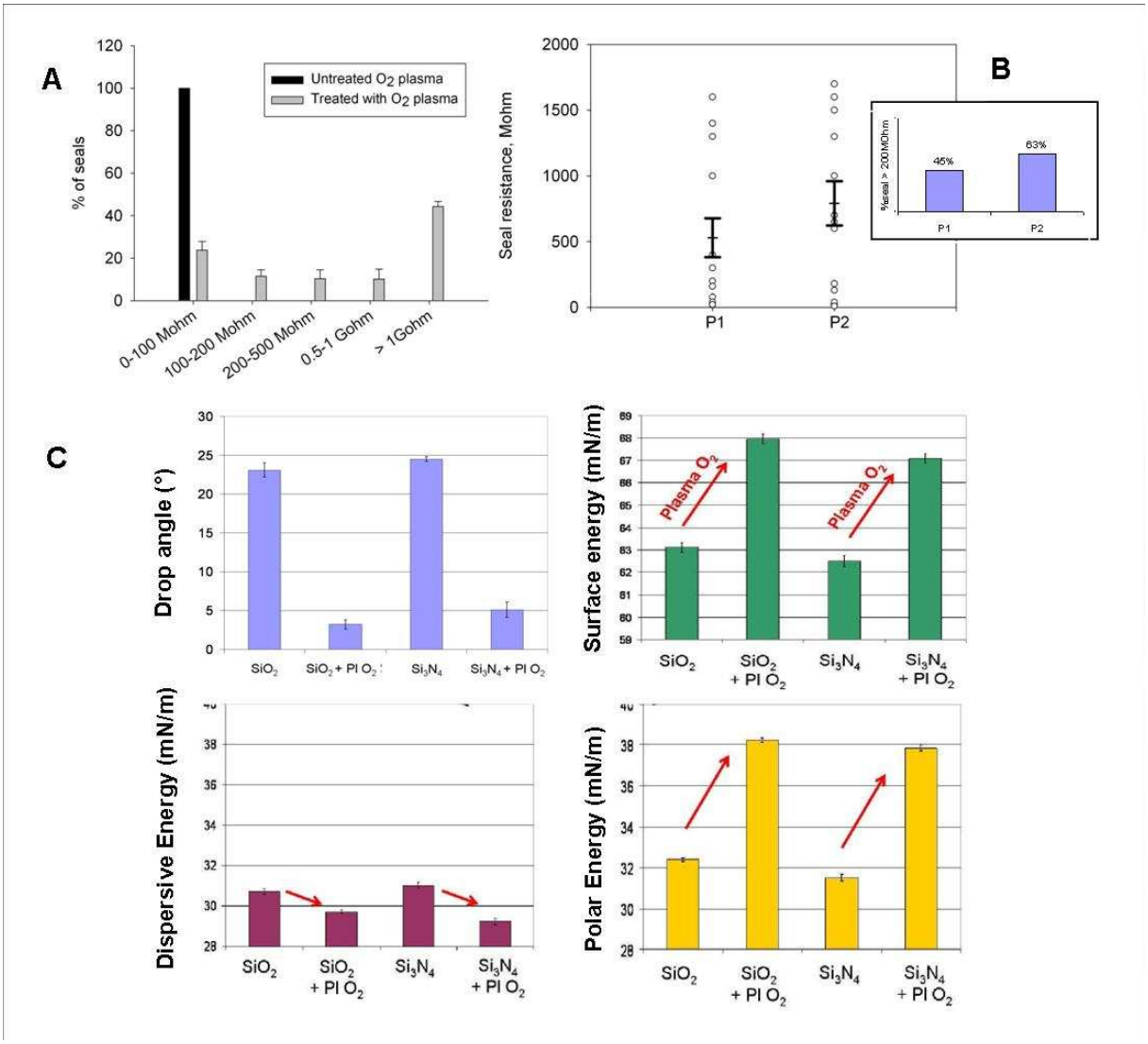
A
% of seals
Untreated O_2 plasma
Treated with O_2 plasma
0-100 Mohm
100-200 Mohm
200-500 Mohm
0.5-1 Gohm
> 1Gohm
B
Seal resistance, Mohm
P1
P2
%seal > 200MOhm
45%
63%
C
Drop angle (°)
Surface energy (mN/m)
Plasma O_2
Dispersive Energy (mN/m)
Polar Energy (mN/m)
SiO_2
SiO_2 + Pl O_2
Si_3N_4
Si_3N_4 + Pl O_2

Figure 3

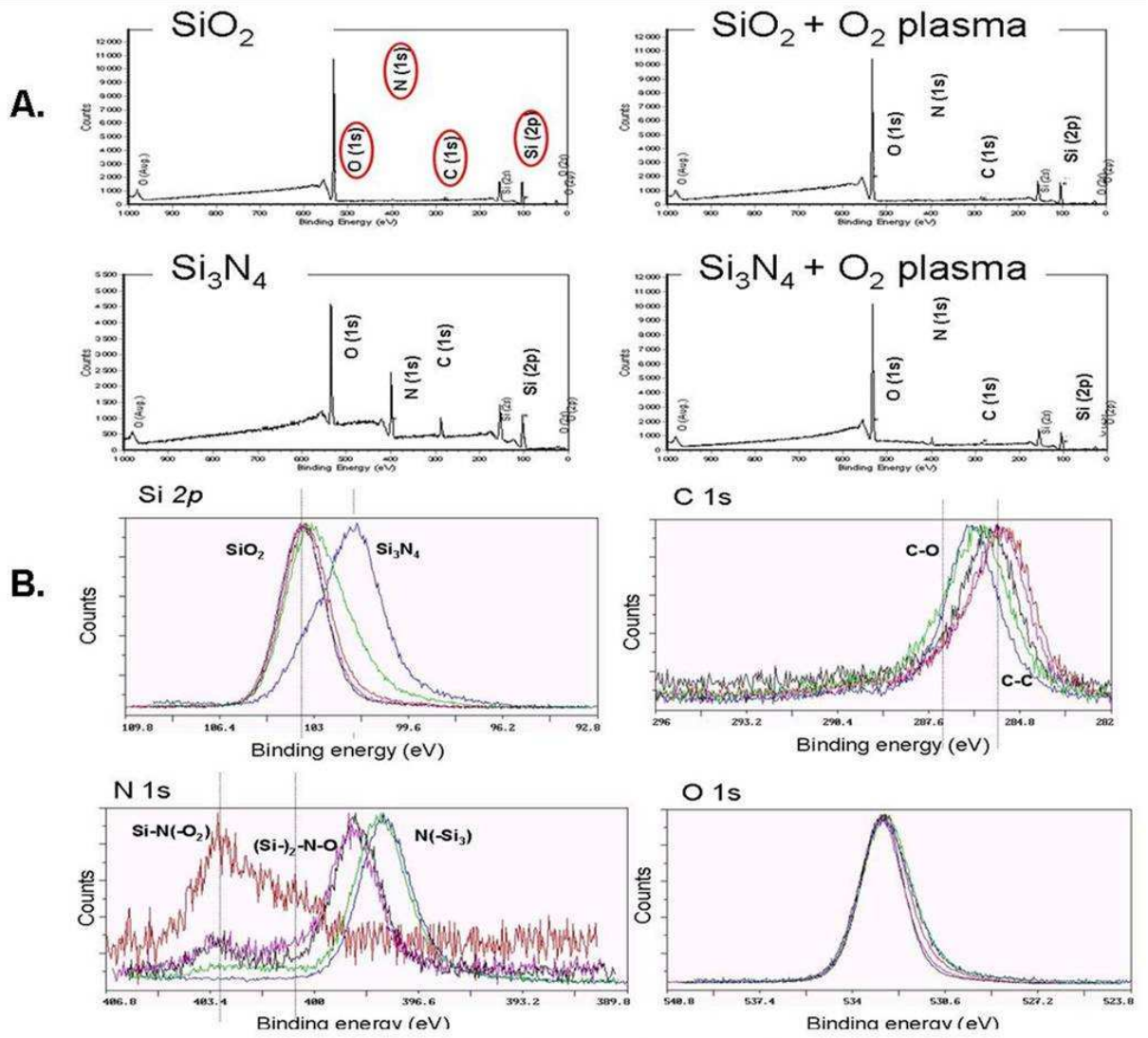

C.

Surface	%Si	%O	%C	%N	Chemical state
SiO_2	30.9	65.1	2.5	1.5	Si-O, C-C, C-O, Si-N(-H_2)
SiO_2 + O_2 plasma	29.3	66.2	3.9	0.6	Si-O, C-C, C-O, Si-N(-O_2)
Si_3N_4	31.8	31.9	9.4	26.9	Si-O, C-C, C-O, N(-Si_3)
Si_3N_4 + O_2 plasma	29.5	61.2	4.8	4.5	Si-O, C-C, C-O, N(-Si_3)

Figure 4

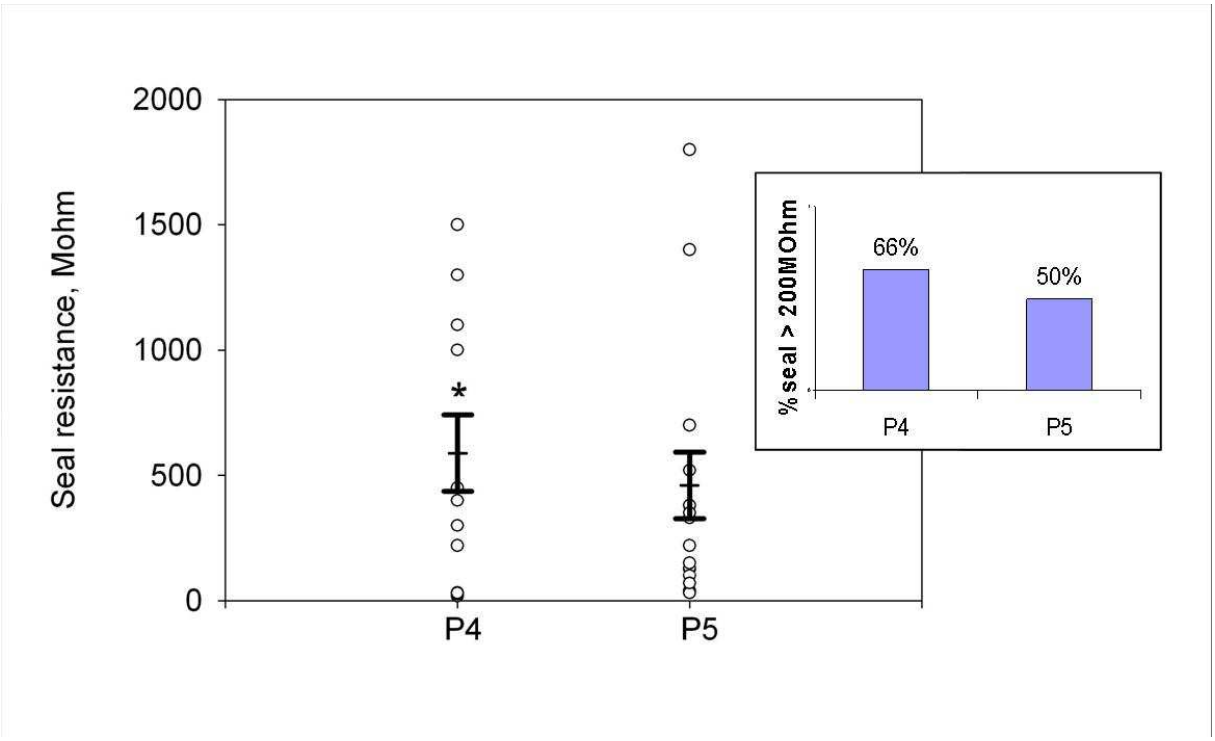
Seal resistance, Mohm
2000
1500
1000
500
0
P4
P5
% seal > 200MOhm
66%
50%
P4
P5

Figure 5

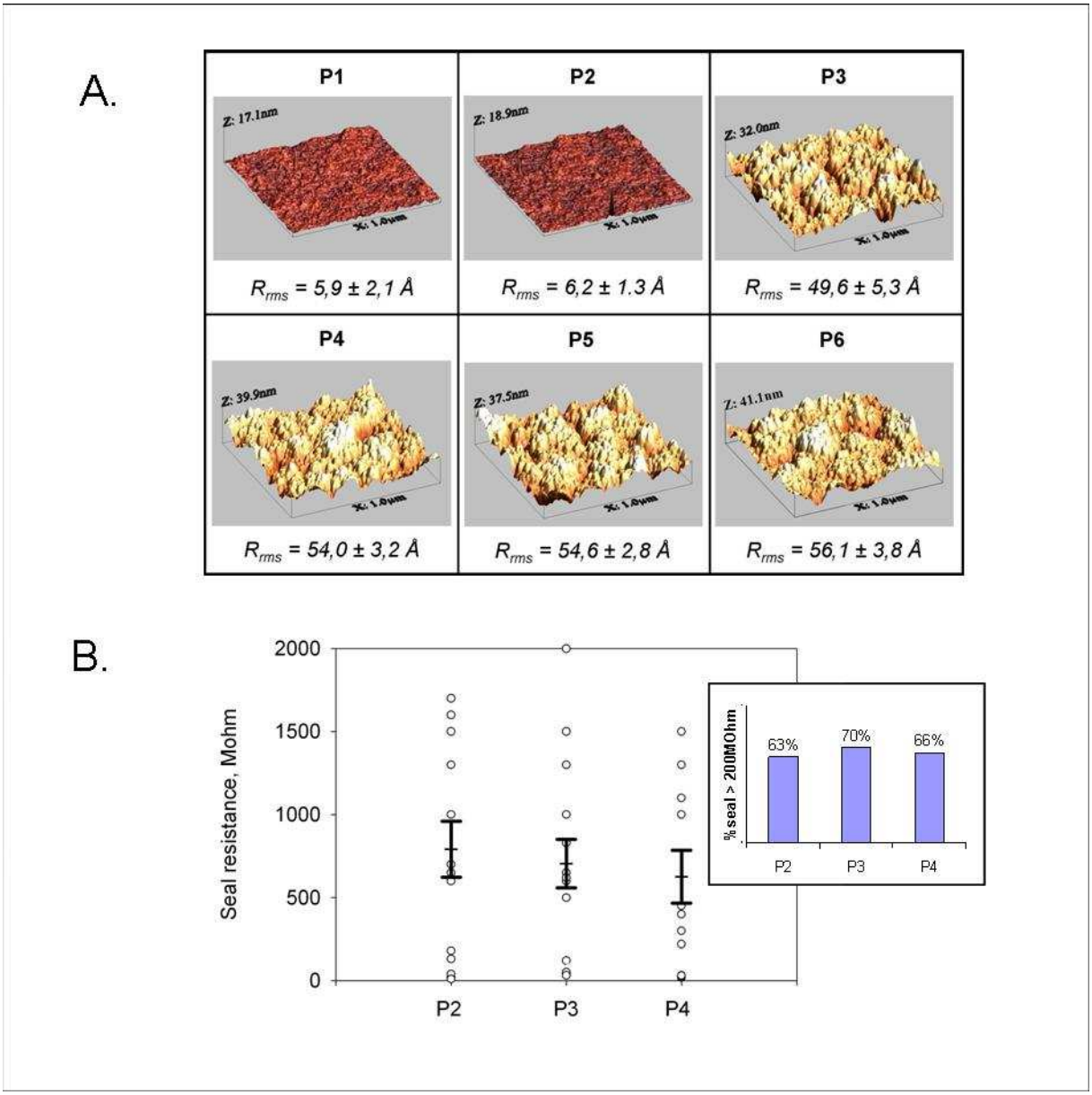
A.
P1
Z: 17.1nm
R_{rms} = 5,9 ± 2,1 Å
P2
Z: 18.9nm
R_{rms} = 6,2 ± 1.3 Å
P3
Z: 32.0nm
R_{rms} = 49,6 ± 5,3 Å
P4
Z: 39.9nm
R_{rms} = 54,0 ± 3,2 Å
P5
Z: 37.5nm
R_{rms} = 54,6 ± 2,8 Å
P6
Z: 41.1nm
R_{rms} = 56,1 ± 3,8 Å
B.
Seal resistance, Mohm
2000
1500
1000
500
0
P2
P3
P4
% seal > 200MOhm
63%
70%
66%
P2
P3
P4

Figure 6

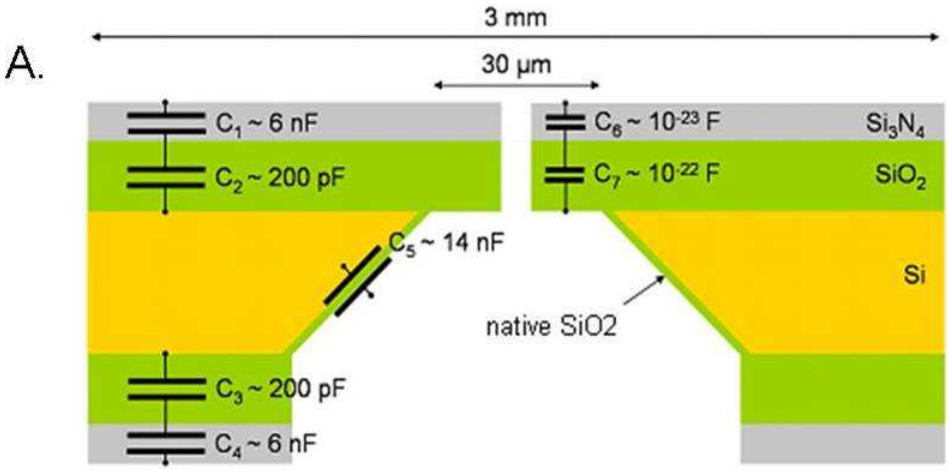

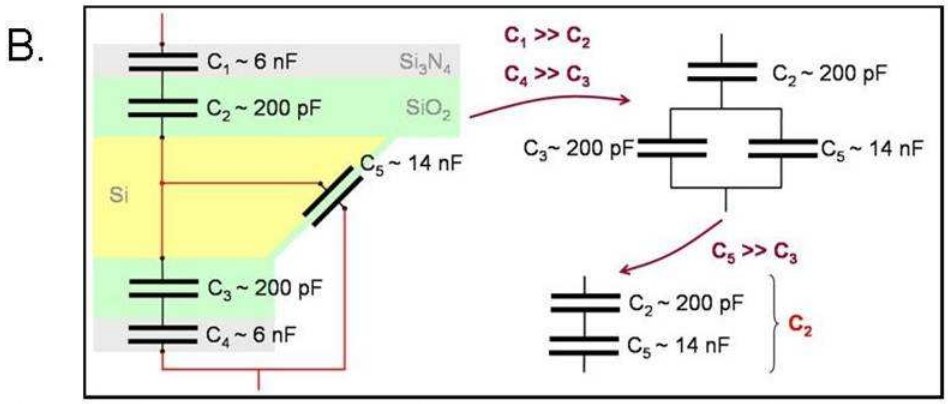

C.

Chip	Top and bottom layers thicknesses	Measured capacitance (pF)	Corrected capacitance (pF)	Theoretical capacitance (pF)
P1	*2 µm SiO2 TEOS +0.12 µm Si3N4 LPCVD*	115 ± 15	110 ± 15	105
P3	*2 µm SiO2 TEOS +0.12 µm Si3N4 LPCVD + 1.5 µm SiO2 PECVD*	54 ± 6	49 ± 6	45
P4	*7 µm SiO2 TEOS +0.12 µm Si3N4 LPCVD + 1.5 µm SiO2 PECVD*	29 ± 4	24 ± 4	20

Figure 7

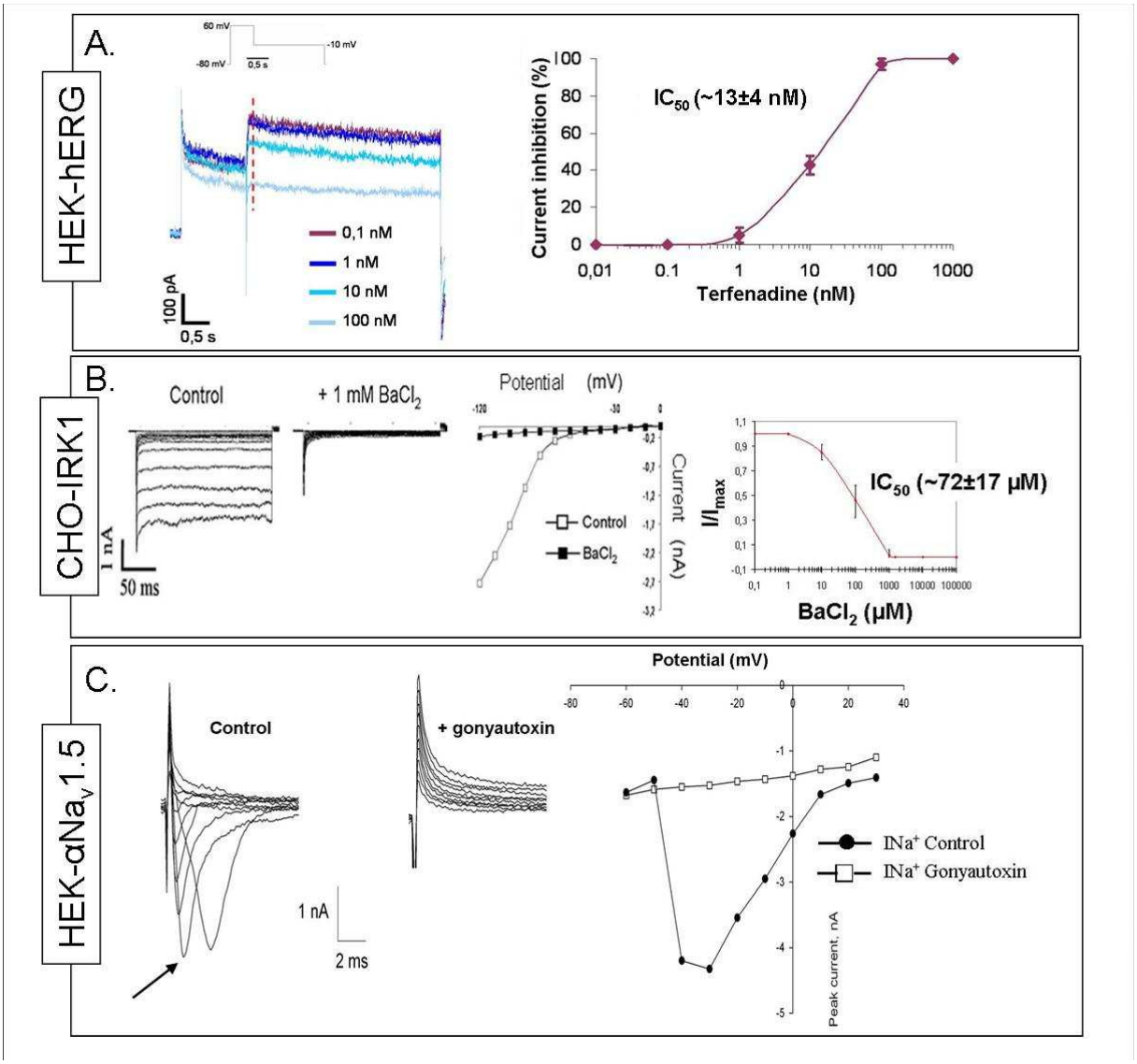
A.
HEK-hERG
60 mV
-80 mV
0,5 s
-10 mV
0,1 nM
1 nM
10 nM
100 nM
100 pA
0,5 s
Current inhibition (%)
IC50 (~13±4 nM)
Terfenadine (nM)
B.
CHO-IRK1
Control
+ 1 mM BaCl2
1 nA
50 ms
Potential (mV)
Control
BaCl2
Current (nA)
I/Imax
IC50 (~72±17 µM)
BaCl2 (µM)
C.
HEK-αNaV1.5
Control
+ gonyautoxin
1 nA
2 ms
Potential (mV)
INa+ Control
INa+ Gonyautoxin
Peak current, nA

Table 1

A.

Variable	Symbol	Coded variable level	
		Low -1	High +1
Microhole diameter (µm)	D	1.8	2.5
Surface roughness (Å)	R	5.9	56.1
Dielectric membrane thickness (µm)	T	2.12	8.72

B.

Method	***Needed parameter***	***Expected information***
SEM	µhole diameter & geometry	Systematic control of the fabricated chip features
AFM	Surface roughness	
Drop angle with water	Surface hydrophily	
Drop angle with 3 liquids	Surface energy, dispersive and polar contributions	Gain insights in the seal formation process
XPS	Atom & binding In the first 5nm layer	

Table 2

Enzyme	Accutase		Trypsin	
Method for cell dissociation	Accumax	Cell mesh	Accumax	Cell mesh
% cell viability at t=0	75		95	
% cell viability at t=1h30	35	70	40	90
% cell viability at t=2h30	25	70	40	90
% cell viability at t=4h30	25	70	35	90
% aggregates before filtration		1		6.5
% aggregates after filtration at t=0		0		0
% aggregates after filtration at t=2h		0		2
% aggregates after filtration at t=4h		0		4